Numerical prediction of cracking risk of reinforced concrete structures at early age

Laurie Lacarriere, Alain Sellier, Pierre Souyris, Batian Kolani, Ponleu Chhun

RILEM Technical Letters (2020) 5: 41-55
https://doi.org/10.21809/rilemtechlett.2020.106

Numerical prediction of cracking risk of reinforced concrete structures at early age: a retrospective view of LMDC's expertise over the last decade

Laurie Lacarriere[1,*], Alain Sellier[1], Pierre Souyris[1], Batian Kolani[1], Ponleu Chhun[1]

[1] Université de Toulouse, UPS, INSA, LMDC (Laboratoire Matériaux et Durabilité des Constructions), Toulouse, France

Received: 19 June 2020 / Accepted: 30 August 2020 / Published online: 24 September 2020

Abstract

The paper presents a summary of the work concerning the prediction of cracking risk in reinforced concrete structures at early age that has been carried out by our team at the LMDC laboratory during the last ten years. It focuses on the principles that must be taken into account in numerical simulations (evolution of characteristics, behaviour law, numerical implementation, effect of reinforcement, etc.) in order to be able to predict the cracking pattern caused in structures by the thermal loading induced by hydration at early ages.

Keywords: Early age; Cracking; Reinforced concrete; Numerical modelling; Heterogeneity; Multi-scale; Steel-concrete bond

1 Introduction

An important aspect of the design and construction specifications for concrete structures is to ensure sufficient service life of the structure.As the durability of the structure over time is strongly conditioned by the possible chemical attacks it may undergo (in particular by a loss of performance with respect to transfers or mechanical properties), the calculation or recalculation of concrete structures can no longer be performed without taking the couplings between the hydro-thermal, chemical and mechanical evolutions of the concrete in the structure into account. This is particularly the case for the state of cracking that can be observed at early age because it can indeed lead to easy propagation of cracks in the long term.

The prediction of this initial state of damage for reinforced concrete structures (generally massive) is accessible through the use of models of physico-chemical and mechanical evolution of cementitious materials that have been developed on a sufficiently macroscopic scale for them to remain applicable to the prediction of the service life of massive structures (bridge piers or segments, dams, containments, radioactive waste storage structures, etc.). The approach developed at the LMDC laboratory over the last few years is based on an approach that is nevertheless intended to be multi-scale, since particular care is taken to observe the hydrate scale in order to understand the phenomena involved and then to transcribe them in terms of evolution laws at the material scale, which can be used in the macroscopic behaviour laws used at the structure scale.

This paper presents the models developed in order to be able to predict the state of early cracking of massive structures subjected to hydration-induced temperature rise with accuracy. The model of the mechanical behaviour of hardening concrete presented here uses the results of hydration, temperature and water content within the structure which are predicted by a multiphysical hydration model not presented here [1].

First, the choice of macroscopic laws of evolution of the mechanical properties is presented, based on a multi-scale study allowing to characterize the properties at a very early age (where few tests are available). The model of non-linear behaviour is then presented, with a detail on the specific numerical adaptations imposed by the evolutionary character of the material induced by hydration. Particular attention is paid to the description of the consideration of the delayed strains and the behaviour of the reinforced concrete as it will be shown that this particularly conditions the cracking pattern of the structures. Finally, it is shown how these models are applied at the scale of a real structure.

* Corresponding author: Laurie Lacarriere, Email: laurie.lacarriere@insa-toulouse.fr

2 Identification of concrete evolution laws used at structural scale

2.1 Cement paste hardening

The progress made at the end of the 1990s in terms of micromechanical characterisation, on a scale small enough to apprehend the properties of cement hydrates, allowed in the 2000s the emergence of calculation methods for estimating the elastic properties of a cement paste based on knowledge of its composition (which can be extracted from hydration models). In particular, analytical homogenisation approaches have been extended to the case of cement paste hardening. For the paste, it is shown that the self-consitent scheme is relevant since it is not really possible to distinguish any inclusion in the paste during structuration. Moreover, this model allows reproducing the solid percolation of the phases [2] . But it is shown that these schemes, although intrinsically taking a solid percolation, led to a strong overestimation of the properties at a very early age for pastes with a W/C ratio lower than 0.5. This overestimation can be reduced in part by considering a localization tensor based on a needle shape of the inclusions [3, 4]. A recent analysis of the evolution of elastic properties continuously measured since the casting (with a technique allowing access to a modulus more comparable to the static modulus than the ultrasonic tests [5]) shows, by inverse analysis, that there is not a single C-S-H morphology allowing to reproduce both the very early age and a more advanced stage of hydration [6]. This indicates that even complex analytical schemes using inclusion forms that are supposed to be more representative of hydrates are therefore questionable when considering the mechanical percolation effect for low W/C ratio pastes.

Another approach consists in taking advantage of numerical microstrutural models (2D or 3D) of hydration in order to perform micromechanical simulations on these REV to extract a homogenized property. We can mention among others the microstructural codes and associated micromechanical models HYMOSTRUC [7, 8], VCCTL based on CEMHYD3D [9, 10] or μic-AIME [11, 12]. A benchmark on these techniques for predicting the properties of cement paste during hydration (analytical and numerical) was recently carried out as part of the European COST TU1404 project [13]. It has been shown that the developments of recent years, in particular for microstructural models and associated micro-mechanical simulations, make it possible to correctly reproduce a good part of the evolution of the elastic properties, but that an overestimation remains significant at low hydration, in particular in comparison with the results of static tests.

Our approaches aim to develop behaviour models that can be used at structural level. They reproduce the non-linear behaviour of concrete (creep, shrinkage, cracking, ...) and all the characteristics of these behaviour laws depend on hydration. The micro-mechanical approaches do not allow for the moment to easily access the evolution of all these characteristics. The modelling of the behaviour of the hardening concrete is thus done by using macroscopic laws of evolution depending only on the hydration degree. In the works presented in this paper, the contribution of analysis at paste scale is to be able to verify the shape of the macro laws for the elastic properties and to identify the macroscopic percolation threshold that will be taken also on the other properties. The choice is therefore made to use a rather simple analytical scheme (self-coherent) for which the percolation consideration is modified in order to consider the effect of the statistical and morphological heterogeneity on the development of hydration.

Before setting, solid particles are not linked by cohesive forces but only by contact forces, so tensile and shear stresses cannot pass through the material interfaces and shear stresses are considerably reduced (if the loading does not have a hydrostatic pressure able to activate friction phenomena) [14, 15]. Our approach considers this aspect by adopting a probabilist function to separate the solid phases of the paste into percolated and non-percolated fractions. The percolated fraction, f_r^P, is defined by the phases that belong to a continuous pathway, where they are bound together by hydration products. This assumption is equivalent to consider a non-perfect hydration rate in the REV, heterogeneity of the hydration rate being explained chemically by the heterogeneous nucleation processes at lower scales. In the present approach, all phases (not only the percolated phases) can transmit compressive stress while only the f_r^P fraction within more hydrated clusters can transmit shear stress. This constitutes another improvement of already existing percolation techniques that consist in assuming that the non-percolated phases have a shear modulus close to zero while their bulk modulus is the same as for the percolated phase (see Fig. 1).

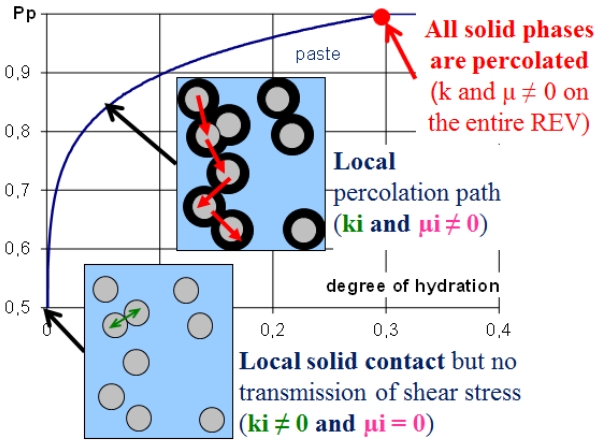

Figure 1. Illustration of percolation function effect on the solid phases of paste (subscript i corresponds to C-S-H, CH, aluminates or anhydrous).

The coherent cluster probability, P_p, increases as the amount of hydrates increases during hydration. This aspect of the function is intuitive and confirmed by numerical simulations in [15, 14]. This percolation function P_p is used to separate solid phases into mechanically percolated and non percolated solid phases (respectively f_r^P and f_r^{NP} in Equation 1).

$$f_r^P = P_p \cdot f_r \quad \text{and} \quad f_r^{NP} = (1 - P_p) \cdot f_r \qquad (1)$$

where:

- f_r is the volume fraction of the solid phase r;
- f_r^P and f_r^{NP} are the percolated and non percolated fractions, respectively, of the solid phase r;
- $\forall r \in$ {anhydrous, portlandite, aluminates, C-S-H HD and C-S-H LD}.

In order to model the cohesive effect created between solid phases by hydrates, the percolation function must depend on the hydration variable (the average hydration degree $\bar{\alpha}$ obtained with a hydration model [16]). As mechanical percolation is obtained more quickly when the solid fraction increases, the positive effect of the presence of initial cluster zones such as aggregates can also be taken into account. As illustrated in Figure 2 the aggregates enable a bridging of the solid phases which gives a percolation greater than that in the paste alone for the same degree of hydration. Since this effect cannot be reproduced using the Mori-Tanaka model (classically used to predict the properties of the mortar from the paste), the percolation function must depend on the quantity of aggregates. For this reason, the aggregate fraction (f_G) is introduced into the percolation function in Equation 2.

$$P_p = min\left\{\left(\frac{\bar{\alpha}}{\bar{\alpha}_p^{cr}(1-f_G)}\right)^m ; 1\right\} \quad (2)$$

where:

- f_G is the volume fraction of aggregates ;
- $\bar{\alpha}_p^{cr}$ and m are material parameters (0.3 and 0.2 respectively for OPC [17]).

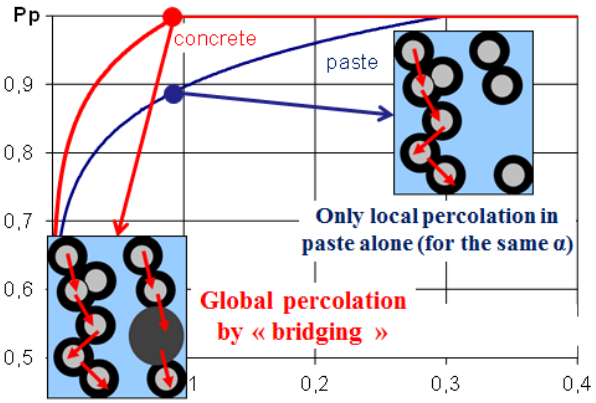

Figure 2. Effect of aggregates on the percolation of paste.

2.2 Implementation of self-consistent scheme with modified percolation for a Portland cement paste

The implementation of this analytical homogenization with consideration of the statistical effect of hydration heterogeneity on percolation requires, like any homogenization method, the knowledge of the elastic properties of the elementary phases considered. It should be remembered that in our approach the solid phases (C-S-H HD and LD, portlandite, aluminates and anhydrous grains) have different shear properties depending on whether they are percolated or not. The properties of the phases issued from the literature (listed in Table 1) are therefore considered for the phases in their percolated state while the shear modulus of the phases is taken equal to 10^{-2} GPa (a null value not being acceptable in the self-coherent homogenization scheme) for non-percolated state.

When applying micro-mechanical homogenization to predict the development of elastic properties during hydration, special attention must be paid to the role of water. At very low hydration degree, it appears that the water movements induced by the deformation of the solid skeleton should be considered. This could only be considered with a true poromechanical formulation that is not easily implementable in micro-mechanical techniques. Idealized conditions should be considered in this case : perfectly drained condition (water compressibility considered equal to zero) or perfectly undrained conditions (compressibility coefficient of water considered). For example, in the case of elastic modulus measurements using ultrasonic techniques [18, 19], we would rather place ourselves in non-drained conditions since the speed of propagation of the acoustic waves does not lead to water drainage. This also partly explains why these measurements give stiffness values that are generally higher than those found in a mechanical test. In the case of a static test, the (relatively low) loading speed makes it possible to assimilate the conditions to drained ones [20, 2, 21] .

Table 1. Micromechanical properties of paste phases (issued from Young's modulus and Poisson's ratio given in [22, 23, 24] for percolated solids.

Phase	k (GPa)	μ_p (GPa)	μ_{np}(GPa)
CH	34.2	15.3	10^{-2}
Aluminates	33.3	15.4	10^{-2}
C-S-H LD	12.8	8.0	10^{-2}
C-S-H HD	19.2	12.1	10^{-2}
Anhydrous grains	112.5	51.9	10^{-2}
Water (undrained)	2.2	10^{-2}	
Water (drained)	10^{-2}	10^{-2}	
Voids	10^{-2}	10^{-2}	

The prediction of the paste microstructure evolution is performed using a multiphasic model of composed binder hydration [1]. The model is applied here to CEM I based pastes but can easily be extended to composed binder as the hydrated phases of this kind of binder are predicted by the multiphasic model [16, 25]. The solid fractions calculated are the ones that compose the paste: anhydrous cement, water, void, portlandite, aluminates (grouping together AFm, ettringite and hexahydrate), and C-S-H gel. The stoichiometry of the created hydrates is supposed to be constant over time and the quantity of hydrates is thus estimated proportionally to the hydration degree of cement according to the following equations (see Table 2). These quantities are expressed according to oxide quantities in the following system of equations (C , S , A , and $\bar{S}$ represents the molar concentration of oxydes in paste (in mol/m^3)).

Table 2. Stoechimoetry hypothesis for portland cement hydration.

Hypothesis 1	Hypothesis 2
if $\boldsymbol{A \geq \bar{S}}$	if $\boldsymbol{A \leq \bar{S}}$
$\partial C_3AH_6/\partial\bar{\alpha} = A - \bar{S}$	$\partial C_3AH_6/\partial\bar{\alpha} = 0$
$\partial C_6A\bar{S}_3H_{32}/\partial\bar{\alpha} = 0$	$\partial C_6A\bar{S}_3H_{32}/\partial\bar{\alpha} = 0.5\bar{S} - 0.5A$
$\partial C_4A\bar{S}H_{12}/\partial\bar{\alpha} = \bar{S}$	$\partial C_4A\bar{S}H_{12}/\partial\bar{\alpha} = 1.5A - 0.5\bar{S}$
$\partial C_{1.7}SH_{2.5}/\partial\bar{\alpha} = S$	
$\partial CH/\partial\bar{\alpha} = C - 1.7S - \bar{S} - 3A$	

The C-S-H gel is sub-divided in high density areas (HD) and low density areas (LD). The amount of LD C-S-H is calculated using a ratio expressed according to the water to cement ratio and to hydration degree (proposed by [26]).

$$\frac{m_{LD}}{m_{C-S-H}} = (3.017 \cdot W/C \cdot \bar{\alpha}) - 1.347\bar{\alpha} + 0.538 \quad (3)$$

The application of this hydration model allows predicting the evolution of paste phases over time for different water-to-cement ratios. These results are presented in Figure 3.

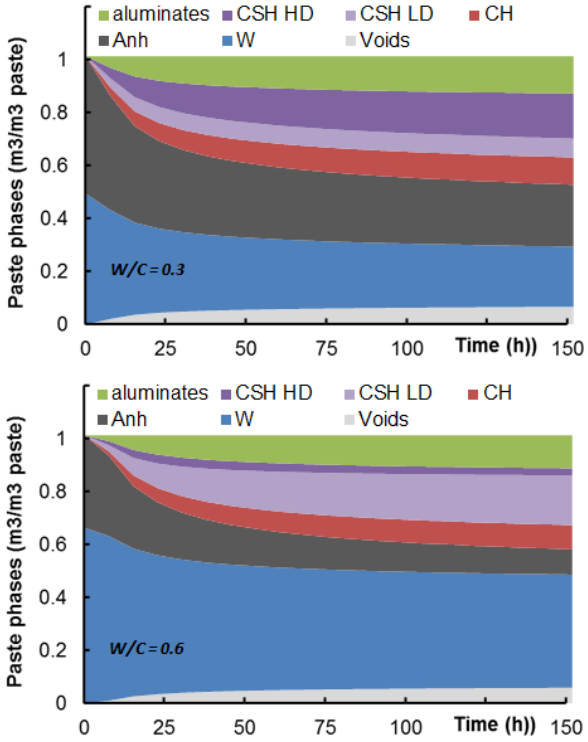

Figure 3. Evolution of paste phases over time for CEM I pastes with W/C = 0.3 and 0.6 (results obtained with the multiphasic hydration model [1]).

Using these hydration results, the solid phases are separated into percolated (able to transmit shear stresses) and non-percolated phases according to Equation 1. Figure 4 illustrates the evolution of solid phases at very early ages. It can be noted that an important part of anhydrous grains are non-percolated (shaded area) during the first hours of hydration. While the global hydration degree is lower than $\bar{\alpha}_p^{cr}$ (0.3 for CEM I cement), a part of the created hydrates is also non-percolated.

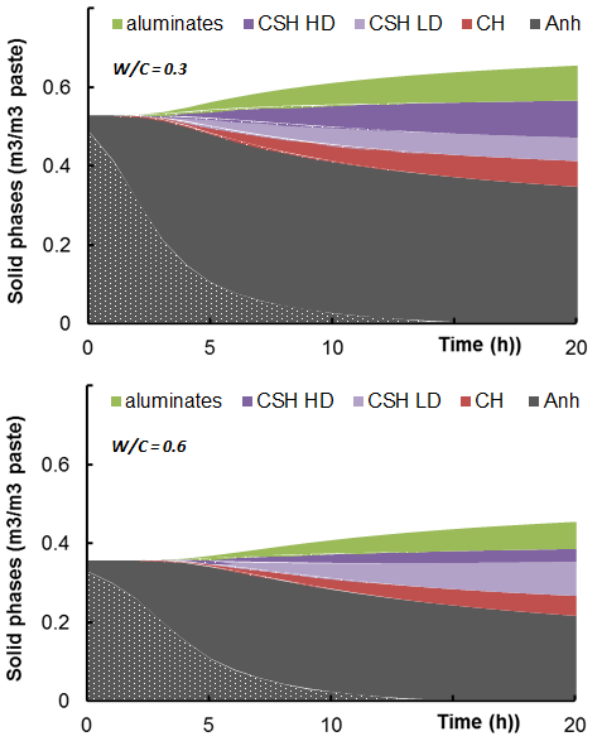

Figure 4. Evolution of percolation of solid paste phases at very early age (shaded areas correspond to the part of the phase that is not percolated).

Applying this percolation approach to the self-consistent model leads to a better estimation of the evolution of the Young's modulus of the paste, including in non-drained conditions for which the self-consistent model (on spherical particles without percolation) greatly overestimates the elastic properties at early age as illustrated on Figure 5 for CEM I pastes with different water-to-cement ratios.

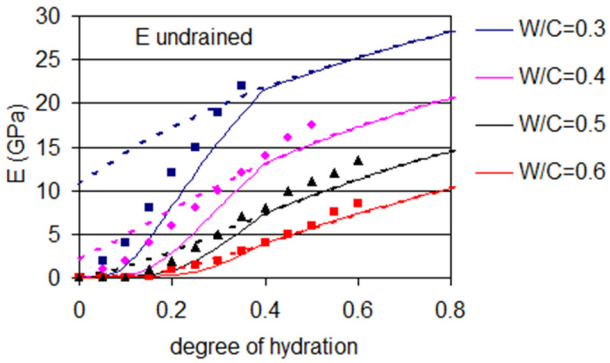

Figure 5. Prediction of the evolution of elastic modulus with percolation law (solid lines) and without (dotted lines) in undrained conditions (experimental measurements from [18]).

2.3 Macroscopic evolution law of mechanical properties for application at structural scale

The interest of such a multi-scale approach is to replace the few experimental results generally available to predict the development of the properties at a very young age and at low hydration levels. The objective is to base the identification of parameters of these macroscopic laws partly on the results of multi-scale approach so as to reduce the number of tests required for parameter determination. Macroscopic laws linking the mechanical properties to a power function of the degree of reaction (equal to 1 at the end of the tests, usually after 1 or 2 months) are commonly used in the literature for ealry age behaviour (before 1 month) [27]. These laws are based on expressing the phenomenon of mechanical percolation [15] in a simple macroscopic way by using a threshold from which the properties start to develop.

In the present study, we propose to express these laws as a function of the average degree of hydration defined from the quantity and stoichiometry of hydrates.

The used hydration model makes it possible to consider an evolution of the mechanical properties even in the long term by chemical reequilibrium between hydrates created at early ages and anhydrous phases (especially for cementitious materials with high ratio of silica) [25]. It is nevertheless more questionable for Portland cement for which ageing can effectively be due to other phenomena than chemical reactions after several months (in this case, equivalent-time is more usually considered), but sufficient for "early age" cracking during the first months. The "degree of hydration concept" also makes it possible to predict in a coupled way the hygro-mechanical evolutions which also play an important role in the risk of cracking (in particular autogenous shrinkage), this would not be possible with equivalent-time formulation.

It is thus proposed to use Equation 4 fitted on the homogenization method given in the last section.

$$X(t) = X_{ref} \cdot \left(\frac{\overline{\alpha}(t)-\overline{\alpha}_s}{\overline{\alpha}_{ref}-\overline{\alpha}_s}\right)^{n_X} \quad (4)$$

where:

- X(t) is the mechanical property at the age considered;
- $\overline{\alpha}(t)$ is the mean hydration degree at this age given by a hydration model (for instance [16, 25]);
- X_{ref} is the mechanical property at a reference age (classically 28 days);
- $\overline{\alpha}_{ref}$ is the mean hydration degree at this same reference age;
- $\overline{\alpha}_s$ is the threshold hydration degree used to model the effect of mechanical percolation. The mechanical properties are null before the hydration degree reaches this threshold;
- n_X is a parameter associated with the mechanical property X (see table 3).

For the parameters associated with Young's modulus, the results of the percolation based homogenization model are used to fit the macroscopic law. The multi-scale model (percolation based homogenization and multiphasic hydration model [1] was used to simulate the development of elastic properties (drained conditions) in paste and the properties of mortar and concrete are predicted using the Mori-Tanaka model considering, as usual, that the matrix is cement paste and the inclusions are sand and aggregates. This method is applied on of 3 different concretes. The results are presented in figure 6 (also compared with static macroscopic tests for 2 concretes). These results show that the same threshold degree can be considered for the 3 concretes (2 ordinary concretes and 1 HPC) and that the exponent $n_E = 0.4$.

It can also be noted that these laws based on an explicit mechanical percolation threshold lead to an overestimation of the modulus between the hydration degrees of 0.2 and 0.4 for concretes.

The threshold hydration degree identified on the elastic properties is then used to simulate the evolution of strengths and fracture energy with the macroscopic law. This identified percolation threshold degree value seems suitable for the resistance results (see Figure 7).

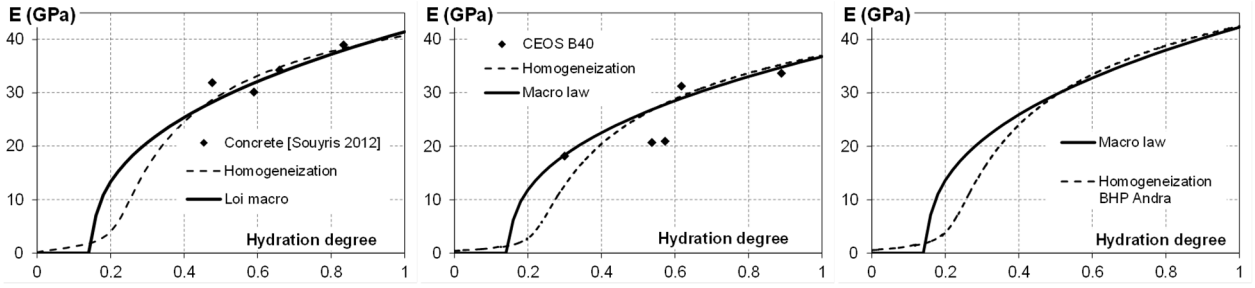

Figure 6. Identification of a macroscopic law for Young's modulus on the results issued given by homogenization technique (dotted curve)(Measurements from [28, 29]).

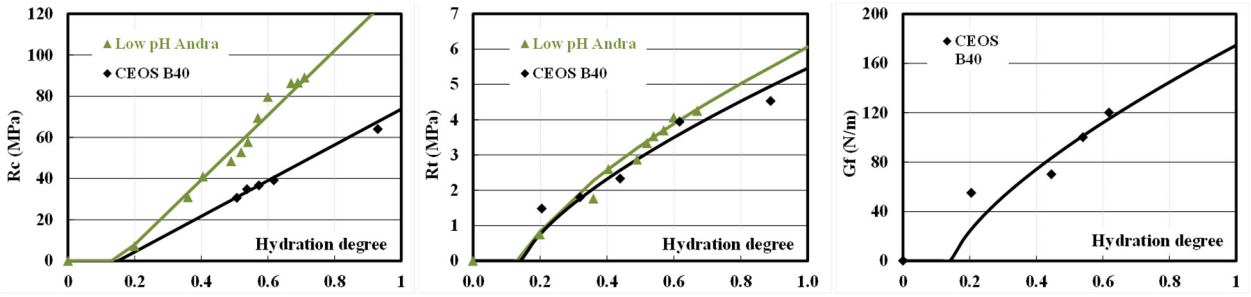

Figure 7. Evolution of strengths and fracture energy according to hydration degree for 2 concretes (Measurements from [29, 30]).

Note that the using same value for n_{Rc}, n_{Rt} and n_{Gf} makes it possible to reproduce the resistance evolution according to hydration for the 3 materials tested, the effect of the type of cement is thus reproduced by the different hydration kinetic. When maturometry tests are not available, the exponent, n_X, and the threshold hydration degree, $\overline{\alpha}_s$, can thus be considered, to be independent to the formulation. The proposed values are reported in Table 2.

Table 2. Parameters of the macroscopic evolution law

$\overline{\alpha}_s$	n_E	n_{Rc}	n_{Rt}	n_{Gf}
0.15	0.4	1	0.7	0.7

In the case of simulations of structures during the design phase, it may be difficult to carry out maturometry tests on the different formulations considered, and the only parameters to be identified will therefore be the characteristics at a given age (28 days for example, values given in Table 3 for the materials tested). In this table, the hydration degree at 28 days $\overline{\alpha_{28j}}$ was determined using the multiphasic hydration model[16] and the values of the property (E, Rc, Rt, gf) at this age was determined on macroscopic static tests.

Table 3. Parameters of the macroscopic evolution law for the different mechanical characteristics.

	C40	CEOS	Low-pH	BHP
$\overline{\alpha_{28j}}$	0.83	0.9	0.57	0.8
E_{28j} (GPa)	38	35	39	-
Rc_{28j} (MPa)	-	65	66	-
Rt_{28j} (MPa)	-	5	3.7	-
Gf_{28j} (MPa)	-	160	-	-

3 Behaviour law for early age reinforced concrete

3.1 Numerical implementation of hardening concrete behaviour law

The calculation of the stress undergone by a cementitious material during hydration is particular: hydration produces new hydrates which appear in a deformed configuration and are free of stress. Therefore the law of behaviour cannot be written in a total differential formulation as in the case of a hardened material. Bazant [31] takes this into account by using the solidification theory. The stress is thus calculated as the integral of the stresses acting on each hydrate, which is a function of the age of formation of the hydrate and the increment of deformation undergone since (Eq. 5).

$$\sigma(t) = \int_{t'=0}^{t} S(t,t') \cdot d\alpha(t') \text{et} S(t,t') = f(\varepsilon(t) - \varepsilon(t')) \quad (5)$$

where:

- t' is the date of hydrate formation;
- S is the stress in the hydrate at time t.

In the case of a total formulation, the total increment of elastic stress $\dot{\sigma}$ applied to a hardening material can be broken down into a part induced by the variation in elastic modulus under constant strain and a part induced by the variation in strain for a constant elastic modulus (Eq. 6).

$$\dot{\sigma} = \dot{E} \cdot \varepsilon + E \cdot \dot{\varepsilon} \quad (6)$$

Based on Bazant's theory of solidification, it can be seen that, as the hydrates newly formed during the time step (thus corresponding to $\dot{E}$) are formed at zero stress ($\varepsilon(t) = \varepsilon(t')$ in Equation 5), the stress increment $\dot{E} \cdot \varepsilon$ is zero.

To take the effect of creep on the mechanical behaviour into account, the effective stress increment $\dot{\tilde{\sigma}}$ is thus calculated in an incremental form, from a rheological model reproducing the delayed behaviour of concrete, as the sum of the increments of the elastic stress applied to the solid skeleton and the stress induced by the capillary pressure increment $\dot{\sigma}^W$ (Eq. 7).

$$\dot{\tilde{\sigma}}_{kl} = S^0_{klmn}(\overline{\alpha}) \cdot \dot{\varepsilon}^{el}_{mn} - \dot{\sigma}^W{}_{kl} \quad (7)$$

$$\dot{\varepsilon}^{el}{}_{mn} = \dot{\varepsilon}_{mn} - \dot{\varepsilon}^{pl}{}_{mn} - \dot{\varepsilon}^{th}{}_{mn} - \dot{\varepsilon}^{Cr}{}_{mn} \quad (8)$$

where:

- S^0_{klmn} is the stiffness matrix (evolving with hydration using Eq. 4);
- $\dot{\varepsilon}_{mn}$ is the total stress increment;
- $\dot{\sigma}^W{}_{kl}$ is the hydric stress increment induced on the solid skeleton by the capillary pressure (see [32] and [33] for more details on this calculation of drying and autodessication consequences in terms of capillary pressure and shrinkage);
- $\dot{\varepsilon}_{mn}$ is the total strain increment;
- $\dot{\varepsilon}^{pl}{}_{mn}$ is the plastic strain increment (from plastic damage model mentioned previously);
- $\dot{\varepsilon}^{th}{}_{mn}$ is the thermal strain increment;
- $\dot{\varepsilon}^{Cr}{}_{mn}$ is the creep strain increment.

3.2 Plasticity and damage model

The mechanical model used, and adapted to carry out the couplings with the physico-chemical evolutions presented here, was developed for hardened concrete and validated in several studies [34, 35, 36, 33]. The total stress, σ_{ij}, is defined

from the effective stress on the hardened material $\tilde{\sigma}_{kl}$(Eq. 9) [34].

$$\sigma_{ij} = \left(1 - D^{\text{shear}}\right) \cdot (1 - D_0^t) \cdot (1 - D^t)_{ijkl} \cdot \tilde{\sigma}^+{}_{kl} + \left(1 - D^{\text{shear}}\right) \cdot R_{ijkl} \cdot \tilde{\sigma}^-{}_{kl} \quad (9)$$

The model thus takes two kinds of damage into account: isotropic damage that models diffuse microcracking, and anisotropic damage that models oriented and localized cracking. The isotropic damage variable is a shear damage variable, D^{shear}, that represents concrete damage induced by compressive stress. It is a function of the associated plastic strain determined with a Drucker-Prager criterion and a pre-peak tensile damage variable, D_0^t, that represents the diffuse microcracking prior to a peak during a tensile stress. It is calculated from the major principal tensile stress.

Anisotropic damage controls the opening (D^t) and reclosing (R) of tensile cracks: Post-peak tensile damage reflects the opening of oriented cracks under tensile stress. It is determined in the main crack base from the maximum crack openings reached, $w^{pl,t,max}$, and a characteristic opening $w^{k,t}$ [37]. The form of the equation was chosen to ensure a finite value of energy (exponent greater than 1) and an adapted form of the softening branch of the law of global behaviour in direct tension.

$$D_I^t = 1 - \left(\frac{w_I^{k,t}}{w_I^{k,t} + w_I^{pl,t,max}}\right)^2 \quad (10)$$

The plastic crack openings are deduced from the plastic tensile strains (themselves calculated from a Rankine criterion).

In addition to the variation of the instantaneous properties managing the occurrence of cracking and its propagation (modulus of elasticity, strengths, fracture energy), taking into account the hydration on the cracking state of the material during hydration also requires a specific update of the internal variables. For mechanical damage, this can be modelled using Equation 11, which leads to a decrease in mechanical damage under the effect of hydration (which then acts as a self-healing process of the cement paste). When the localized tensile damage, D^t, decreases under the effect of hydration, the crack opening $w^{k,t}$ is recalculated by inverting Equation 10 (some details can be found in [38]).

$$\frac{\partial D^t}{\partial \bar{\alpha}} = -\frac{D^t}{\bar{\alpha}} \quad (11)$$

Finally, in the case of finite element applications, it should be noted that the local damage pattern is energy-regularized. The crack opening is calculated from the length of the finite element l_I so that the energy dissipated during the local damage remains equal to the tensile cracking energy G_f^t (Eq. 12).

$$G_f^t \approx l_I \frac{(R^t)^2}{2E\left(1 - D_0^t\right)} + R_I^t w_I^{pl,t,max} \quad (12)$$

In the case of application to massive structures, the regularization method can lead to a post-peak branch in tension that is too brittle (or even a snap-back) on large finite elements (especially if l_I is such that $w_I^{pl,t,max}$ becomes negative in Equation 12). In order to avoid the convergence problems inherent in this, a modified cracking energy is introduced to ensure a minimum slope of the descending branch. An error variable is then constructed, allowing the zones to be re-meshed more finely if the error made on the cracking energy is not acceptable.

3.3 Creep model for hardening concrete

It might seem rather contradictory to speak of deferred deformations in the study of the short-term behaviour of a material but these visco-elastic deformations play an important role in the global behaviour of structures whose deformations at a young age are partially or totally blocked. If the development of stress is determined in a restrained concrete tie subjected to a thermal evolution corresponding to hydration, the results presented in Figure 8 are obtained (black curve obtained by an incremental elastic calculation and red curve by a calculation taking incremental creep and shrinkage into account). We can see that, if we neglect the delayed deformations, we obtain an overestimation of the stresses during the heating phase, which leads to tensile stresses being obtained later if creep is neglected and, consequently, to delayed cracking.

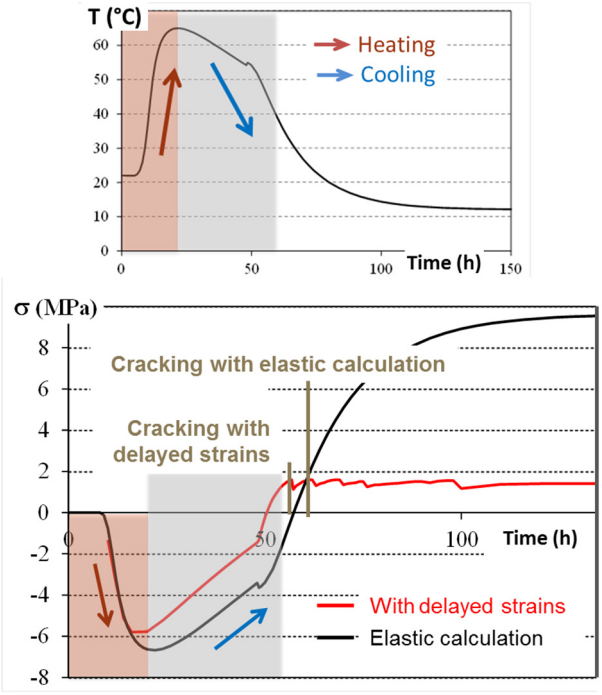

Figure 8. Effect of delayed strain consideration in the calculation of the stress and cracking risk of a restrained concrete tie at early age.

To take account of the creep effect on the mechanical behaviour, the effective stress increment $\dot{\tilde{\sigma}}$ is calculated as the sum of the increments of the elastic stress applied to the solid skeleton and the stress induced by the capillary pressure increment $\dot{\sigma}^W$ (Eq. 7). The creep model used in this work was a nonlinear viscoelastic model based on a reversible Kelvin ε^{Kl} viscoelastic part and a consolidating Maxwell ε^M viscoelastic part [33].

$$\dot{\varepsilon}_{mn}^{Cr} = \dot{\varepsilon}_{mn}^K + \dot{\varepsilon}_{mn}^M \quad (13)$$

Kelvin's model handles the deformation of the reversible stage reproducing the short-term creep of concrete associated with capillary water movement. (Eq. 14).

$$\dot{\varepsilon}^K_{mn} = \frac{1}{\tau^K(T,W)}\left(\frac{\varepsilon^{el}_{mn}}{\psi^K} - \varepsilon^K_{mn}\right) \quad (14)$$

where:

- $\tau^K(T,W)$ is the characteristic time considering the effect of water saturation and temperature on creep rate (see [33] for more details);
- ψ^K is the Kelvin modulus.

The non-linear Maxwell modulus models the deformation of the consolidating viscous stage, reproducing the permanent creep associated, among others, with the viscous sliding of the C-S-H sheets [39, 33] (Eq. 15).

$$\dot{\varepsilon}^M_{IJ} = \frac{\varepsilon^{el}_{IJ}}{\tau^M_{ref}\min(C^C_I, C^C_J)} \quad (15)$$

where:

- I, J are the principal directions of Maxwell strains;
- τ^M_{ref} is the Maxwell characteristic time;
- C^C is the consolidation coefficient calculated according to the strain ε^M following Equation 16.

$$C^C_I = \frac{1}{k^M(T,W)} \cdot \exp\left(\frac{1}{k^M(T,W)}\left(\frac{\varepsilon^M_I}{\varepsilon^{el}_{II}}\right)^+\right) \quad (16)$$

where:

- $k^M(T,W)$ models the non-linearity of creep rate according to the stress, and its dependence on the temperature and the water content [33].

The creep model presented is formulated so that the creep rates and amplitudes are direct functions of the elastic properties of the material (through the dependence on ε^{el} in Equations 14 and 15). The dependence on hydration is thus taken into account through the evolution of the elastic properties previously detailed. This implicit dependence assumes that the characteristic times of creep rates are not affected by hydration, which has been used by various authors [40, 41]. However, like the damage variable, the internal variables associated with consolidation affecting the viscosity of the non-linear Maxwell stage are updated as a function of the degree of hydration, leading to a progressive deconsolidation of the material, which was subjected to high viscous deformation at a low degree of hydration. Furthermore, in order to remain compatible with hydration, it must be considered that the new hydrates are created in the deformed configuration and are therefore free of stress [31]. The elastic deformations of the ε^{el} and Kelvin ε^K elastic stages must therefore be updated (and managed as internal variables of the creep model) in order to reproduce the decrease in elastic deformation at the macroscopic scale under the effect of the creation, at the microscopic scale, of hydrates in the deformed configuration without associated elastic stress.

The creep-damage model briefly presented previously had been used to perform a parametric study highlighting the influence of taking creep into account on a restrained reinforced concrete tie (2% steel) subjected to the same temperature evolution (note that the model was validated in previously published papers by confrontation with experimental results [32]). The obtained numerical results for this parametric study are presented in Figure 7 (in terms of global response), and show a slightly larger opening of the main crack with the effect of creep (Figs. 8 and 9).

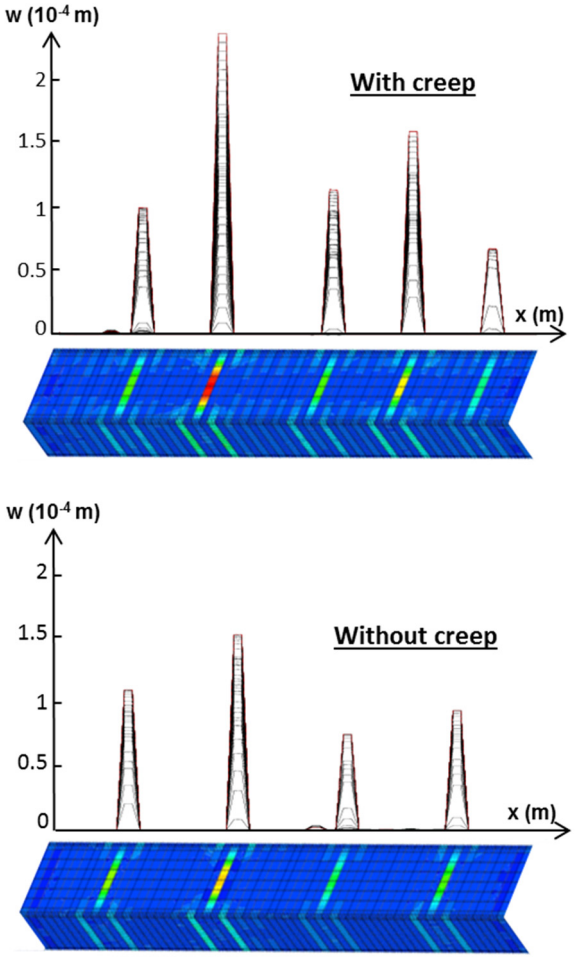

Figure 9. Cracking pattern and crack opening in the restrained tie when creep is considered or not.

3.4 Model behaviour for reinforced concrete

3.4.1 Steel-concrete bond at early age

The modelling of the steel-concrete interface is a subject widely covered in the literature for hardened concretes with formulations and developments adapted for the prediction of the behaviour of reinforced concrete structures.

The most widespread approach is based on surface [42, 43, 44] or linear [45, 46] elements. The steel bar and the surrounding concrete are connected by a steel stress vector with a stiffness matrix or kinematic relationships. For these approaches, although the overall bonding behaviour of the steel-concrete interface is well reproduced, this can lead to pathological effects of mesh dependence due to the concentration of stresses at the singularity that can lead to an artificial deterioration of the concrete around the bar.

This risk of stress concentration can be avoided by volumetric modelling of the interface. Several authors have implemented this approach [47, 48] with varying degrees of complexity. [47] for example explicitly considers the ribs of the reinforcing bar to take into account the heterogeneity properties of the steel-concrete interface, but this approach is difficult to apply to large-scale structures because of the explicit complexity of the required mesh and the associated computational time.

The approach adopted in this work to model the evolution of the behaviour of reinforced concrete was to use a volumetric interface element between finite element bar and concrete elements. The behaviour of this volumetric interface is elasto-plastic with negative strain-hardening that occupies the real volume of the reinforcement and through the centre of which a bar element having the properties of steel is modelled.

The model developed is a non-associated elasto-plastic model with isotropic strain-hardening based on a Drucker-Prager criterion whose initial cohesion, C_0, and strain-hardening modulus, H, will depend on hydration. This dependence allows reproducing the progressive mobilization of reinforcement through the steel-concrete interface that manages the cracking pattern.

In order to determine the evolution of the initial cohesion, C_0, and the isotropic strain-hardening modulus, H, as a function of hydration, pull-out tests were carried out at different ages. The parameters C_0 and H were determined by inverse analysis by numerical modelling of pull-out tests performed at the ages of the tests. The dilation angle, which also controls the Drucker Prager criterion, is, as a first approximation, assumed to be independent of hydration. It is determined for a reference age of 28 days from the strength of the concrete.

The model was then tested on the prediction of a pulling test carried out at an age that was intermediate among the ages used for the identification of the evolution laws (degree of hydration of 0.6) and the results presented in Figures 10 and 11 show that ageing the elasto-plastic interface law makes it possible to reproduce the behaviour of this mini-structure.

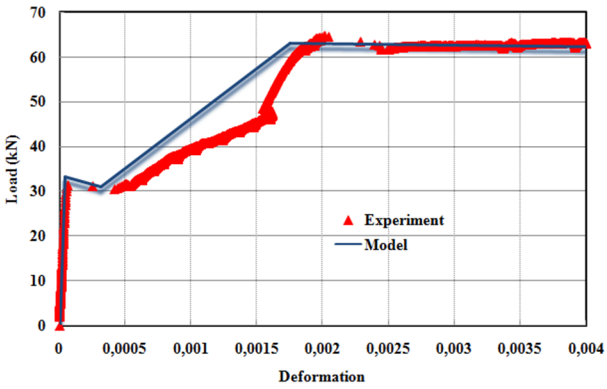

Figure 10. Force-displacement curve for direct tensile test on concrete prism.

3.4.2 Identification of the effect of reinforcement on early age cracking pattern

The effect of reinforcement on the risk of cracking at early age was investigated by numerical parametric studies on virtual structures that had been subjected to the same thermal history. The concrete was the same as that used in the CEOS project [49] and the thermal boundary conditions were idealized (constant outside temperature, no solar flux, insulation and formwork on all sides removed 48 hours after pouring). The model used was the one presented in this paper and which had been validated on the real structures of the CEOS project (see [32]). The "virtual" modelled structures were concrete anchors whose extremities were thermally insulated even after the formwork had been removed from the running part in order to reproduce the effect of embedding these anchors in massive structural elements (see Figure 12).

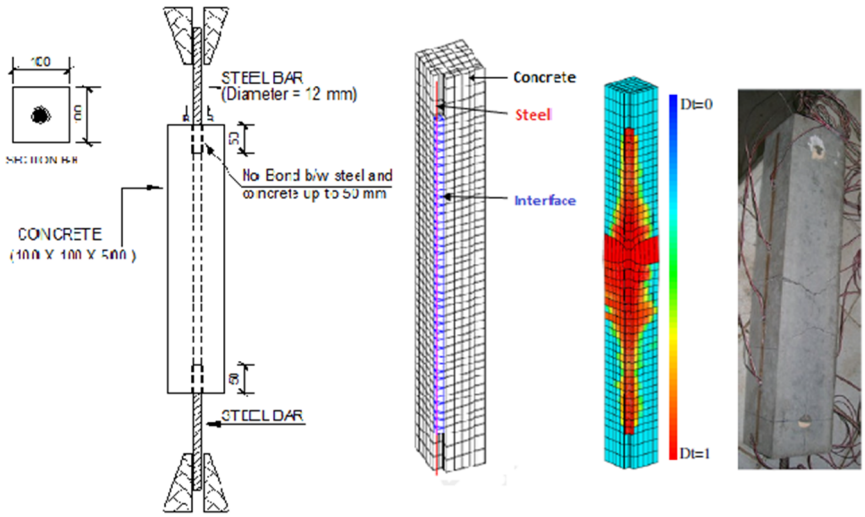

Figure 11. Cracking pattern obtained at the end of the test.

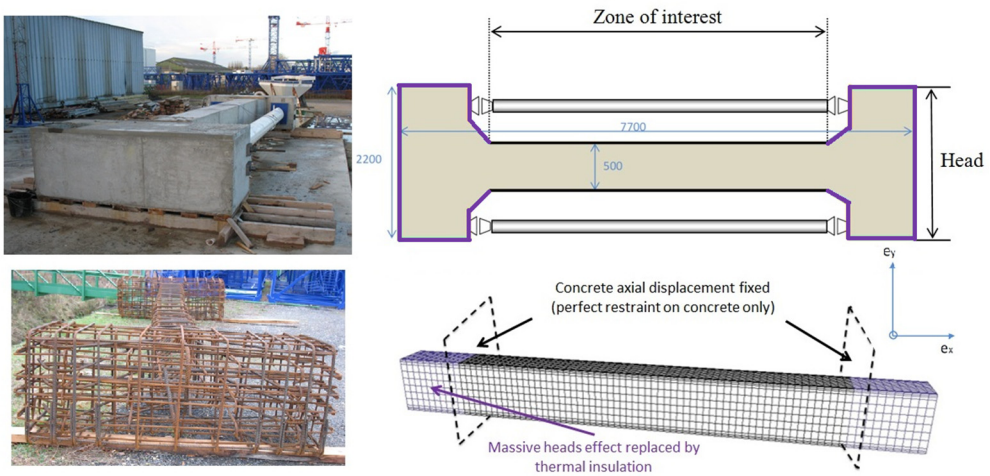

Figure 12. Geometry and mechanical boundary conditions of virtual restrained structures (VS).

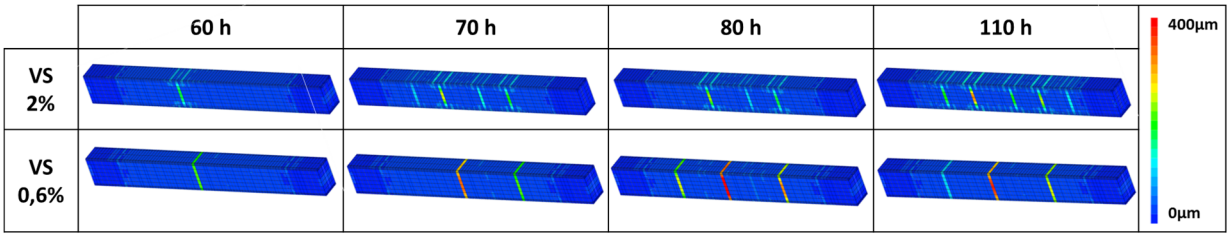

Figure 13. Effect of reinforcement ratio on cracking pattern.

The simulations were first performed on two virtual structures: one with a reinforcement ratio of 2 % and a 30 mm coating (VS 2%) and the other with a steel ratio of 0.6 % and a 30 mm coating (VS 0.6%). For both structures, the first crack was obtained 56 hours after casting (during the cooling period) and the cracking pattern evolved until 150 hours after casting (see Fig. 13)(the temperature was equilibrated with the environment in the structure at approximately 100 hours).

First of all, it can be seen that the reinforcement does not influence the moment of appearance of the first localized crack. As expected, a decrease in the rate of reinforcement leads (from VS 2% to VS 0.6%) to fewer but more open cracks. We also note that, in this case, the cracks (initiated through the core) are not stopped by the reinforcement bed in the case of low reinforcement ratio (VS 0.6%) and propagate to the surface, whereas they spread after the reinforcement bed for the higher reinforcement rate (VS 2%).

From the numerical simulation, we can also observe the development of stresses during cracking development. It can be seen in Figure 14 (which represents the evolution of the stress distribution in the reinforcement and in the concrete from casting to 56 hours for the virtual structure with 2% of steel) that compressive stresses develop in the steel during the heating of the concrete. In this structure (as can be the case on structures where the steel bars are anchored in a more massive area) the extremities of the tie are subjected to a greater temperature rise and therefore to a faster development of the mechanical properties of the concrete. The steel therefore anchors quickly at its ends, thus blocking its thermal deformation in the anchorage zone. Figure 14 also shows that the first crack occurrence leads to a stress transfer from the concrete to the steel over 80 cm on both sides of the crack.

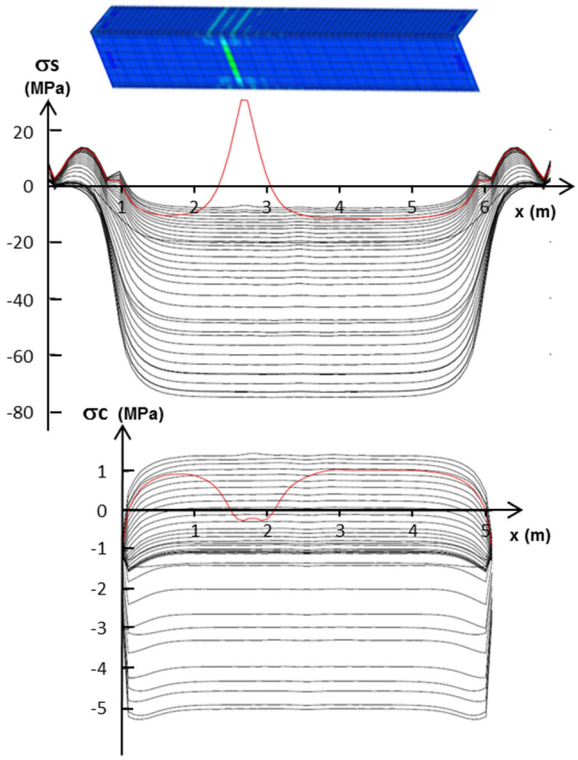

Figure 14. Stress profiles along the tie length (VS 2%) in the reinforcement and in concrete over time (red curves obtained at the 1st crack occurrence, 56 h after casting).

It should be noted that the same conclusions can be drawn from the simulation performed on the virtual structure with 0.6% of steel (before the first crack).

These profiles of stress evolution in the reinforcement can be drawn during the entire cracking development for both structures. Figure 15 presents these evolutions from casting to 140 hours after casting for both reinforcement ratios.

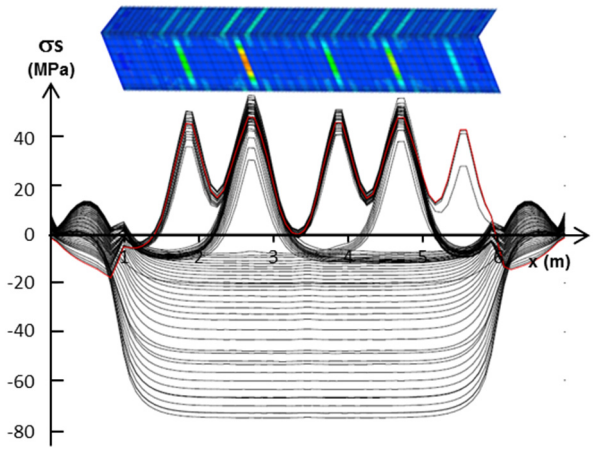

Figure 15. Stress profiles along the tie length (VS 2%) in the reinforcement over time (red curve obtained at the occurrence of the 5th crack, 140 h after casting).

It can be observed that the steel remains compressed even when the concrete is put under tension and during the first crack (outside the crack anchoring zone), and that it is necessary to wait for a high density of localized and open cracks (as observed at 140 h) to obtain tension in the entire tie.

Finally, we can also look at the effect of reinforcement on the shear stress profile developed in the interface at the time of cracking (and thus when loads are transferred from concrete to reinforcement). Figure 16 shows this profile along the lower main reinforcement in both structures 130 hours after casting, i.e. when the cracking is stabilized.

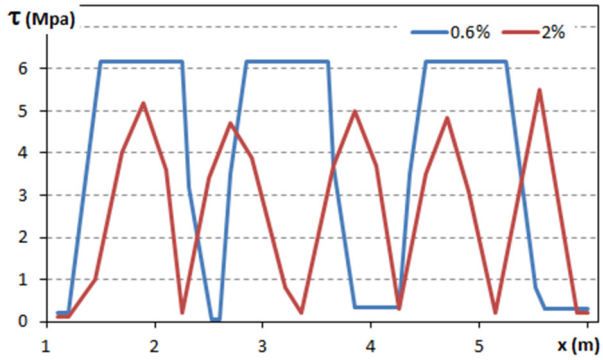

Figure 16. Effect of reinforcement ratio on the distribution of shear stresses for the structures with two steel ratio.

It can be seen that, for the least reinforced structure (VS 0.6%), there is indeed a plastification of the interface with a constant shear stress in the zone of reanchoring of the steel around the crack (as is classically the case in the regulatory calculations). On the other hand, for the most reinforced case (VS 2%), due to more numerous and less open cracks, the stress developed in the interface does not reach the plastic limit. The interface therefore remains in the elastic domain and the stress evolves linearly in the steel reanchoring zone.

4 Application of hardening concrete mechanical model at structural scale

The applicability of the hardening mechanical model developed for concrete at real structure scale required some specific scientific developments, in particular to account for the scale effect on the tensile strength of concrete (highlighted by the structural tests of the national CEOS project [49]). This phenomenon of a decrease in strength as the volume of concrete increases is known as the Weibull scale effect, based on the theory of the weakest link and therefore a greater probability of encountering this weak link in a larger volume [50, 51].

This effect has been experimentally studied with direct tensile tests carried out on concretes of strength classes ranging from 30 to 130 MPa [52], and it has been shown that the scale effect decreases with increasing strength class. This effect can then be represented by Weibull's law linking the decrease in tensile strength to the ratio between concrete volumes. This theory has been adapted by Sellier [53], who linked the decrease in resistance to the ratio of the volumes loaded in traction (and not the geometrical volumes). Moreover, in order to avoid the tensile strength tending towards zero for large volumes, he proposed limiting the volume to be considered (V_{eq} in Equation 17) to a maximum volume related to a characteristic length identified at 1.2 m [53].

$$\frac{Rt}{Rt_{ref}} = \left(\frac{V_{ref}}{V_{eq}}\right)^{1/m} \quad (17)$$

where:

- Rt_{ref} is the tensile strength measured on a reference specimen for which the volume V_{ref} is subjected to tensile stress ($V_{ref} = 242cm^3$ in the case of a Brazilian test on a 11 cm diameter and 22 cm height specimen);
- V_{eq} is the volume subjected to tensile stress (limited according to a characteristic length used in the modelling of probabilistic heterogeneity [53]);
- m is the Weibull exponent calculated according to the variation coefficient on experimental results (C^v).

$$m \approx \frac{1}{10}\left(\frac{12}{C^v} - 2\right) \quad (18)$$

If the mechanical test results available are not available to determine the coefficient of variation C^v, the value of the Weibull coefficient can be estimated from the compressive strength [52] (Equation 19).

$$m = (0.25 - 3.6E^{-3} \cdot Rc + 1.3E^{-5} \cdot Rc^2)^{-1} \quad (19)$$

Since the equivalent volume V_{eq} is dependent on the tensile stress state of the material, the tensile strength is not an

intrinsic quantity and has be evaluated during the calculation. This is achievable in the finite element solver Cast3M ([54] developped by CEA) by a non-local calculation based on [53]. However, for a simplified approach it can be calculated as the product of the dimensions of the estimated area subjected to tensile stress, each dimension being limited to a length of 1.2 m. [55] (determined in connection with the above-mentioned non-local calculation). This effect is illustrated in Figure 17 for 4 concretes of different strength classes. The values calculated for several structures representative of structures presenting a risk of cracking at a early age are given.

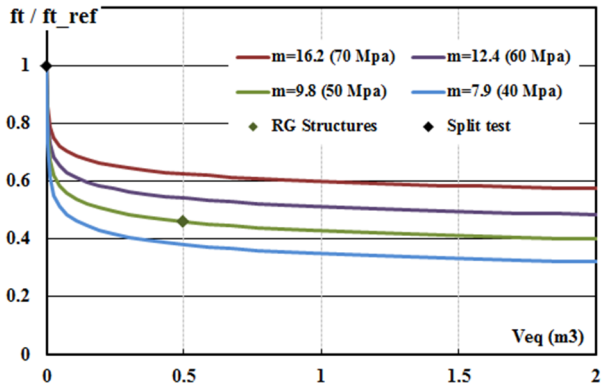

Figure 17. Scale effect for different concrete classes.

It can thus be seen that, for restrained ties such as those used in the parametric study, as the entire tie is under tension during the cooling of the structure, the resistance to be taken into account is equal to 46% of the resistance determined by splitting (green curve on Figure 17 evaluated with a coefficient m of 9.8), which corresponds to the experimentally observed drop in resistance [49]. If we consider a very massive restrained structure for which the dimension of tensile zone during cooling at young age is greater than 1.2 m in all 3 directions, the equivalent volume will be equal to $(1.2m)^3$ and the tensile strength could, for example, be between 32% and 57% of the strength measured in splitting (for strength classes from 40 to 70 MPa).

For thinner structures, e.g. a wall whose deformations are blocked by the support on which it is cast, it is known that the tensile stresses will first develop in the skin, due to the thermal gradient (leading to surface cracking), and then in the core during global cooling (leading to through cracking). In this case, for a 1.2 m thick wall such as the Civaux experimental wall, we can see that the tensile strength to be considered for the risk of surface cracking is estimated at 60% of the cracking strength while, for through cracking, it is 50%.

This technique has been applied to predict the early behaviour of the inner vessel of the Vercors model (a 1/3 scale model of a containment vessel), where it was applied within the framework of our participation in the international benchmark study organized by EDF on this subject [56]. More specifically, the aim was to assess the strains and cracking pattern of the lower part of the vessel (gusset + lower part of the wall) during the first few weeks after casting. The geometry of the mock-up and of the part of the structure studied in this work are shown in Figure 18.

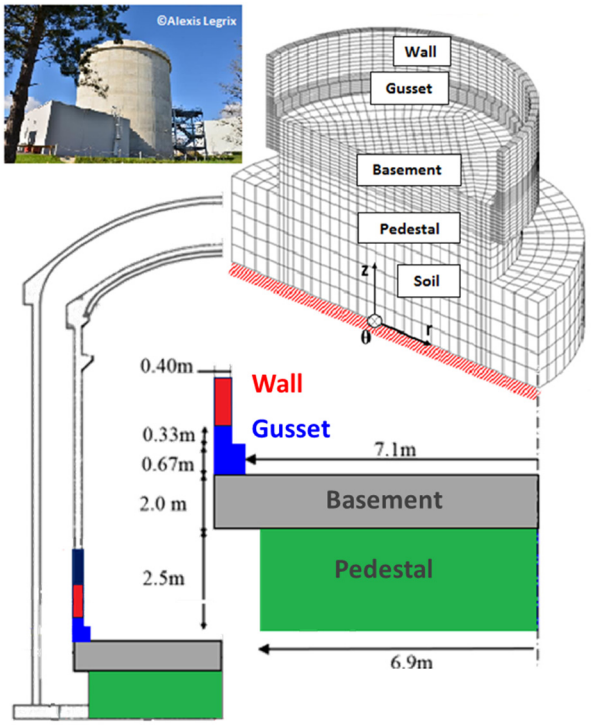

Figure 18. Geometry of Vercors mock-up and details on the gusset and mesh used for the simulation (only a half is presented but the entire structure was meshed and calculated)..

The numerical results obtained using the model at the temperature measurement points are compared with the experimental measurements in Figures 19 and 20. It can be seen that the numerical results are in line with the measurements, which makes it possible to approach the modelling of the mechanical behaviour of the gusset at early age with confidence.

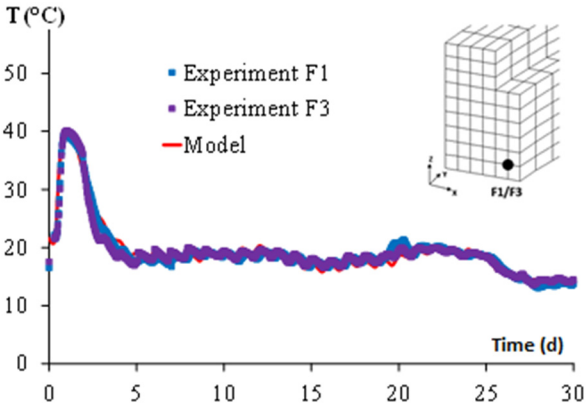

Figure 19. Temperature obtained by the model on inner face on the gusset.

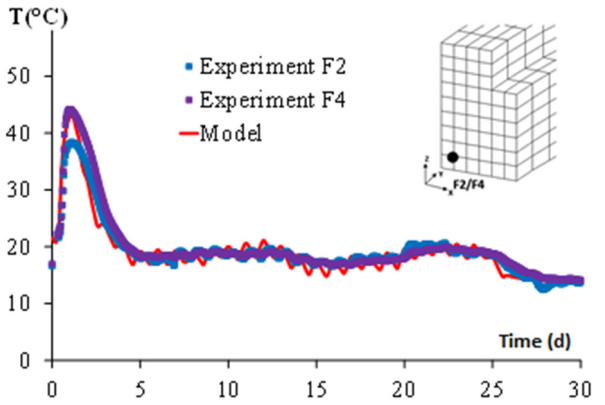

Figure 20. Temperature obtained by the model on outer face on the gusset.

The mechanical simulation was run on the complete structure (up to the 2nd lift) from the casting of the slab (taking into account the hardened pedestal, see Figure 18 which shows only half the structure for visibility reasons).

The mechanical calculation at early age was carried out considering the modelling of the only passive reinforcement because the prestressing was not active at the construction stages studied. It is obvious that, when the aim is to predict the risk of cracking in the Vercors mock-up, explicit modelling of the reinforcement and steel-concrete interfaces, as carried out on the structures of the CEOS project, is unrealistic given the size of the structure and the high rate of reinforcement (in the 3 directions). The choice was therfore made to use homogenized modelling of the reinforced concrete by considering the reinforcements as inclusions in the REV with the method developed in [38]. It is based on a non-local formulation that considers, in the homogenized element, the effect of steel-concrete sliding within the REV on the reinforcement strain.

The scale effect was also taken into account. The Weibull exponent was calculated from the coefficient of variation obtained on tensile strength measurements carried out in the framework of Macena project ([57]). The model having been instrumented and monitored in terms of cracking pattern, it was possible to compare the numerical results with the behaviour of the structure in situ. It can be seen on Figure 21 that the total deformations (thermal + mechanical) are well reproduced by the model. This result is presented in an uncracked section (experimentally and numerically).

Figure 22 allows a comparison with the results obtained in situ as cracking was measured on the internal and external faces of the gusset over the entire circumference of the mock-up 5 days after the gusset was cast.

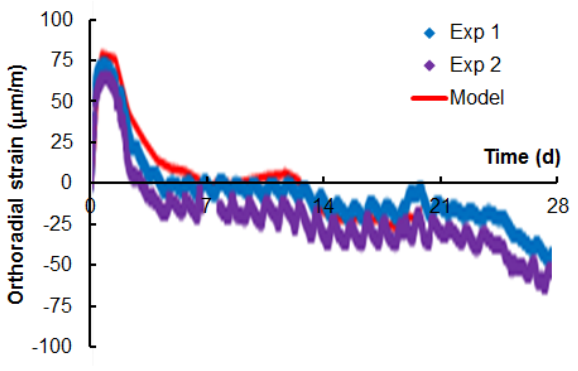

Figure 21. Orthoradial strains on inner face.

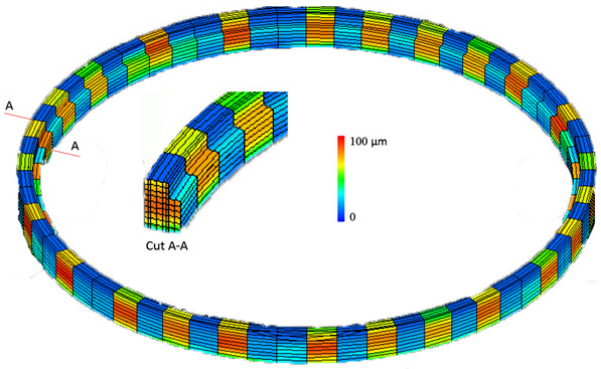

Figure 22. Cracking pattern (with opening) on the gusset obtained with the model 5 days after its casting.

Experimentally, about 15 to 20 cracks with openings ranging from 50 μm to 100 μm were observed on both sides. A large proportion of the cracks were facing each other, and therefore assumed to be through cracks. The cracks exhibited a cumulative opening over the entire circumference of about 800 to 1500 μm. Numerically more cracks were observed, since we counted 25 cracks with openings all less than 100 μm on the surface, for a cumulative opening on the surface of about 2000 μm. The similarity of the results is therefore acceptable given the lack of knowledge of certain parameters (characterization of tensile strength during hydration, creep test at young age, etc.), and certain boundary conditions (homogeneity of gusset heating along the circumference).

5 Conclusion

To realistically predict the risk of cracking of a reinforced concrete structure at early age, several important phenomena must be taken into consideration. First of all, the mechanical percolation threshold must be predicted as accurately as possible. To do this, it is not sufficient to use of a conventional homogenization method because the heterogeneous aspect of hydration within the REV used in the homogenization scheme leads to non-homogeneous percolation. A way of considering this first level of heterogeneity has been proposed. It consists of a probabilistic method combined with the self-consistent homogenization scheme. Secondly, at the macroscopic level, a differential formulation of the elastic behaviour is necessary and the viscous behaviour cannot be neglected. Otherwise there is a

risk of compressive stress during the heating period, followed by an overestimation of tensile stress during the cooling period (in the case of restrained structures). Thirdly, the progressive anchorage of the steel bars must be considered in order to obtain a realistic prediction of re-anchoring after the first crack. Prediction of early crack spacing is therefore dependent on a law of early interface behaviour being taking into account. Finally, the probabilistic scaling effect cannot be neglected for large structures since it can lead to a reduction of about 50% in tensile strength relative to laboratory cracking tests.

6 Acknowledgements

The studies reported in this paper were partially funded by the French National Research Agency (ANR and ANR-PIA) under the research programmes *CEOS.fr*, *Mefisto* and *MACENA* (11-RSNR-0012 Control of nuclear vessel in accident conditions).

The authors also acknowledge the technical and financial support of the French Group *VINCI Construction Grands Projets* and particularly thank *Laurent Boutillon* and *Lionel Linger* from the Scientific Department for their collaboration and expertise.

We are finally grateful to *CEA/DEN/DM2S/SEMT* for providing the finite element code *Cast3M*.

7 References

[1] L. Buffo-Lacarriere, A. Sellier, G. Escadeillas, A. Turatsinze, Multiphasic finite element modeling of concrete hydration, Cem Concr Res (2007) 37(2): 131-138. https://doi.org/10.1016/j.cemconres.2006.11.010

[2] O. Bernard, F.J. Ulm, E. Lemarchand, A multiscale micromechanics-hydration model for the early-age elastic properties of cement-based materials. Cem Concr Res (2003) 33(9): 1293-1309. https://doi.org/10.1016/S0008-8846(03)00039-5

[3] J. Sanahuja, L. Dormieux, G. Chanvillard, Modelling elasticity of a hydrating cement paste. Cem Concr Res (2007) 37(10): 1427-1439. https://doi.org/10.1016/j.cemconres.2007.07.003

[4] [4] B. Pichler, C. Hellmich, Upscaling quasi-brittle strength of cement paste and mortar: A multi-scale engineering mechanics model. Cem Concr Res (2011) 41(5): 467-476. https://doi.org/10.1016/j.cemconres.2011.01.010

[5] M. Azenha, R. Faria, F. MagalhÃ£es, L. Ramos, Ã. Cunha, Measurement of the E-modulus of cement pastes and mortars since casting, using a vibration based technique. Mater Struct (2012) 45(1): 81-92. https://doi.org/10.1617/s11527-011-9750-9

[6] C.F. Dunant, J. Granja, A. Muller, M. Azenha, K.L. Scrivener, Microstructural simulation and measurement of elastic modulus evolution of hydrating cement pastes. Cem Concr Res (2020) 130: 106007. https://doi.org/10.1016/j.cemconres.2020.106007

[7] K. Van Breugel, Simulation of hydration and formation of structure in hardening cement-based materials. PhD Thesis, 1991.

[8] Z. Sun, G. Ye, S.P. Shah, Microstructure and early-age properties of Portland cement paste - Effects of connectivity of solid phases. ACI Mater J (2005): 102(2): 122-129. https://doi.org/10.14359/14306

[9] D.P. Bentz, CEMHYD3D: A Three-Dimensional Cement Hydration and Microstructure Development Modeling Package. Version 3.0, 2005. https://doi.org/10.6028/NIST.IR.7232

[10] L. Valentini, M. Parisatto, V. Russo, G. Ferrari, J.W. Bullard, R.J. Angel, M.C. Dalconi, G. Artioli, Simulation of the hydration kinetics and elastic moduli of cement mortars by microstructural modelling. Cem Concr Compos (2014) 52: 54-63. https://doi.org/10.1016/j.cemconcomp.2014.05.005

[11] S. Bishnoi, K.L. Scrivener, Âµic: A new platform for modelling the hydration of cements. Cem Concr Res (2009) 39(4): 266-274. https://doi.org/10.1016/j.cemconres.2008.12.002

[12] C.F. Dunant, E.C. Bentz, Algorithmically imposed thermodynamic compliance for material models in mechanical simulations using the AIM method. Int J Num Meth Eng (2015) 104(10): 963-982. https://doi.org/10.1002/nme.4969

[13] M. Wyrzykowski, J. Sanahuja, L. Charpin, M. Königsberger, C. Hellmich, B. Pichler, L. Valentini, T. Honório, V. Smilauer, K. Hajkova, G. Ye, P. Gao, C. Dunant, A. Hilaire, S. Bishnoi, M. Azenha, Numerical benchmark campaign of COST Action TU1404 - microstructural modelling. RILEM Tech Lett (2017) 2: 99-107. https://doi.org/10.21809/rilemtechlett.2017.44

[14] L. Stefan, F. Benboudjema, J.M. Torrenti, B. Bissonnette, Prediction of elastic properties of cement pastes at early ages. Comput Mater Sci (2010) 47(3): 775-784. https://doi.org/10.1016/j.commatsci.2009.11.003

[15] J.M. Torrenti, F. Benboudjema, Mechanical threshold of cementitious materials at early age. Mater Struct (2005) 38(3): 299-304. https://doi.org/10.1007/BF02479294

[16] B. Kolani, L. Buffo-Lacarriere, A. Sellier, G. Escadeillas, L. Boutillon, L. Linger, Hydration of slag-blended cements. Cem Concr Compos (2012) 34(9): 1009-1018. https://doi.org/10.1016/j.cemconcomp.2012.05.007

[17] P. Souyris, Prediction des proprietes poro-elastiques et de sorption d'eau en fonction du developpement de la microstructure des materiaux cimentaires. PhD Thesis, Universite de Toulouse, Universite Toulouse III - Paul Sabatier, France (2012)

[18] A. Boumiz, C. Vernet, F. Cohen Tenoudjit, Mechanical properties of cement pastes and mortars at early ages. Advn Cem Bas Mater (1996) 3: 94-106. https://doi.org/10.1016/S1065-7355(96)90042-5

[19] M. Bourissai, F. Meftah, N. Brusselle-Dupend, e. Lecolier, G. Bonnet, Evolution of the Elastic Properties of an Oilwell Cement Paste at Very Early Age under Downhole Conditions: Characterization and Modelling. Oil & Gas Science and Technology – Rev IFP Energies nouvelles (2013) 68(3): 595-612. https://doi.org/10.2516/ogst/2012087

[20] V. Baroghel-Bouny, M. Mainguy, T. Lassabatere, O. Coussy, Characterization and identification of equilibrium and transfer moisture properties for ordinary and high-performance cementitious materials, Cem Concr Res (1999) 29(8): 1225-1238. https://doi.org/10.1016/S0008-8846(99)00102-7

[21] T. Rougelot, F. Skoczylas, N. Burlion, Water desorption and shrinkage in mortars and cement pastes: Experimental study and poromechanical model. Cem Concr Res (2009) 39(1): 36-44. https://doi.org/10.1016/j.cemconres.2008.10.005

[22] P.J.M. Monteiro, C.T. Chang, The elastic moduli of calcium hydroxide. Cem Concr Res (1995) 25(8); 1605-1609. https://doi.org/10.1016/0008-8846(95)00154-9

[23] K. Velez, S. Maximilien, D. Damidot, G. Fantozzi, F. Sorrentino, Determination by nanoindentation of elastic modulus and hardness of pure constituents of Portland cement clinker. Cem Concr Res (2001) 31(4), 555-561. https://doi.org/10.1016/S0008-8846(00)00505-6

[24] G. Constantinides, F.J. Ulm, The effect of two types of C-S-H on the elasticity of cement-based materials: Results from nanoindentation and micromechanical modeling. Cem Concr Res (2004) 34(1): 67-80. https://doi.org/10.1016/S0008-8846(03)00230-8

[25] Y. El Bitouri, L. Buffo-Lacarriere, A. Sellier, X. Bourbon, Modelling of chemo-mechanical behaviour of low pH concretes, Cem Concr Res (2016) 81: 70-80. https://doi.org/10.1016/j.cemconres.2015.12.005

[26] P.D. Tennis, H.M. Jennings, A model for two types of calcium silicate hydrate in the microstructure of Portland cement pastes. Cem Concr Res (2000) 30(6): 855-863. https://doi.org/10.1016/S0008-8846(00)00257-X

[27] G.D. Schutter, L. Taerwe, Degree of hydration-based description of mechanical properties of early age concrete, Mater Struct (1996) 29(6): 335. https://doi.org/10.1007/BF02486341

[28] L. Buffo-Lacarriere, Prevision et evaluation de la fissuration precoce des ouvrages en beton. PhD Thesis, Universite de Toulouse, INSA de Toulouse, France, 2007.

[29] B. Kolani, Comportement au jeune age des structures en beton arme a base de liants composes avec laitiers. PhD Thesis, Universite de Toulouse, Universite Toulouse III - Paul Sabatier, France, 2012.

[30] T. Leung Pah Hang, Les betons bas pH : comportements initial et differe sous contraintes externes. PhD Thesis, Universite de Toulouse, Universite Toulouse III - Paul Sabatier, France, 2015.

[31] Z.P. Bazant, S. Prasannan, Solidification theory for aging creep, Cem Concr Res (1998) 18(6): 923-932. https://doi.org/10.1016/0008-8846(88)90028-2

[32] L. Buffo-Lacarriere, A. Sellier, B. Kolani, Application of thermo-hydro-chemo-mechanical model for early age behaviour of concrete to

experimental massive reinforced structures with strain-restraining system. Eur J Env Civ Eng (2014) 18(7): 814-827. https://doi.org/10.1080/19648189.2014.896754
[33] A. Sellier, S. Multon, L. Buffo-Lacarriere, T. Vidal, X. Bourbon, G. Camps, Concrete creep modelling for structural applications: non-linearity, multi-axiality, hydration, temperature and drying effects. Cem Concr Res (2016) 79: 301-315. https://doi.org/10.1016/j.cemconres.2015.10.001
[34] A. Sellier, G. Casaux-Ginestet, L. Buffo-Lacarriere, X. Bourbon, Orthotropic damage coupled with localized crack reclosure processing. Part I: Constitutive laws. Eng Fract Mech (2013) 97: 148-167. https://doi.org/10.1016/j.engfracmech.2012.10.012
[35] A. Sellier, G. Casaux-Ginestet, L. Buffo-Lacarriere, X. Bourbon, Orthotropic damage coupled with localized crack reclosure processing. Part II: Applications. Eng Fract Mech (2013) 97: 168-185. https://doi.org/10.1016/j.engfracmech.2012.10.016
[36] A. Sellier, L. Buffo-Lacarriere, Towards a simple and unified modelling of basic creep, shrinckage and drying creep of concrete, Eur J Env Civ Eng (2009) 13(10): 1161-1182. https://doi.org/10.1080/19648189.2009.9693184
[37] A. Sellier, Anisotropic Damage and Visco-Elasto-Plasticity Applied to Multiphasic Materials. report, LMDC - Laboratoire Materiaux et Durabilite des Constructions de Toulouse ; Universite de Toulouse III - Paul Sabatier ; INSA de Toulouse, 2018.
[38] A. Sellier, A. Millard, A homogenized formulation to account for sliding of non-meshed reinforcements during the cracking of brittle matrix composites: Application to reinforced concrete. Eng Fract Mech (2019) 213: 182-196. https://doi.org/10.1016/j.engfracmech.2019.04.008
[39] P. Acker, F.J. Ulm, Creep and shrinkage of concrete: physical origins and practical measurements. Nucl Eng Des (2001) 203(2): 143-158. https://doi.org/10.1016/S0029-5493(00)00304-6
[40] F. Benboudjema, J.M. Torrenti, Early-age behaviour of concrete nuclear containments. Nucl Eng Des (2008) 238(10): 2495-2506. https://doi.org/10.1016/j.nucengdes.2008.04.009
[41] G. De Schutter, Degree of hydration based Kelvin model for the basic creep of early age concrete. Mater Struct (1999) 32(4): 260. https://doi.org/10.1007/BF02479595
[42] F. Ragueneau, N. Dominguez, A. Ibrahimbegovic, Thermodynamic-based interface model for cohesive brittle materials: Application to bond slip in rc structures. Comput Methods Appl Mech Eng (2006) 195: 7249-7263. https://doi.org/10.1016/j.cma.2005.04.022
[43] A. Millard, M. Vivier, Modelling of tests performed in order to evaluate the residual strength of corroded beams in the framework of the benchmark of the rance beams. Journal de Physique IV (Proceedings) (2006) 136: 151-158. https://doi.org/10.1051/jp4:2006136016
[44] Finite element modelling of reinforcement with bond. Comput Struct (2006) 84(28): 1780-1791. https://doi.org/10.1016/j.compstruc.2006.04.010
[45] C. Mang, L. Jason, L. Davenne, A new bond slip model for reinforced concrete structures: Validation by modelling a reinforced concrete tie. Eng Comput (2015) 32: 1934-1968. https://doi.org/10.1108/EC-11-2014-0234
[46] A. Casanova, L. Jason, L. Davenne, Bond slip model for the simulation of reinforced concrete structures, Eng Struct (2007) 39: 66-78. https://doi.org/10.1016/j.engstruct.2012.02.007
[47] A. Michou, A. Hilaire, F. Benboudjema, G. Nahas, P. Wyniecki, Y. Berthaud, Reinforcement concrete bond behavior: Experimentation in drying conditions and meso-scale modeling. Eng Struct (2015) 101: 570-582. https://doi.org/10.1016/j.engstruct.2015.07.028
[48] R. Hameed, A. Sellier, , A. Turatsinze, F. Duprat, Simplified approach to model steel rebar-concrete interface in reinforced concrete, KSCE J Civ Eng (2017) 21: 1291-1298. https://doi.org/10.1007/s12205-016-1397-1
[49] L. Buffo-Lacarriere, S. Baron, F. Barre, D. Chauvel, A. Darquennes, J.P. Dubois, J. Gayete, F. Grondin, B. Kolani, H. Lancon, others, Restrained shrinkage of massive reinforced concrete structures: results of the project CEOS. Fr. Eur J Env Civ Eng (2016) 20(7): 785-808. https://doi.org/10.1080/19648189.2015.1072587
[50] Z.P. Bazant, A. Yavari, Is the cause of size effect on structural strength fractal or energetic-statistical? Eng Fract Mech (2005) 72(1): 1-31. https://doi.org/10.1016/j.engfracmech.2004.03.004
[51] A. Carpinteri, B. Chiaia, G. Ferro, Size effects on nominal tensile strength of concrete structures: multifractality of material ligaments and dimensional transition from order to disorder. Mater Struct (1995) 28(6): 311. https://doi.org/10.1007/BF02473145
[52] P. Rossi, X. Wu, F. Lemaou, A. Belloc, Scale effect on concrete in tension. Mater Struct (1994) 27(172): 437-444. https://doi.org/10.1007/BF02473447
[53] A. Sellier, A. Millard, Weakest link and localisation WL2: a method to conciliate probabilistic and energetic scale effects in numerical models. Eur J Env Civ Eng (2014) 18(10): 1177-1191. https://doi.org/10.1080/19648189.2014.906368
[54] CEA. Finite element solver Castem. http://www-cast3m.cea.fr/. Accessed September 2020.
[55] F. Barre, P. Bisch, D. Chauvel, J. Cortade, J.P. Dubois, S. Erlicher, E. Gallitre, P. Labbe, J. Mazars, C. Rospars, A. Sellier, J.M. Torrenti, F. Toutlemonde, Control of cracking in reinforced concrete structures. ISTE Ltd/John Wiley and Sons Inc, Hoboken, NJ, 2016. https://doi.org/10.1002/9781119347088
[56] P. Chhun, L. Buffo-Lacarriere, A. Sellier, Material and Geometric Heterogeneity Consideration for Cracking Risk Prediction of Young Age Behavior of Experimental Massive Reinforced Concrete Structure. Key Eng Mater (2016) 711: 900-907. https://doi.org/10.4028/www.scientific.net/KEM.711.900
[57] P. Chhun, Modelisation du comportement thermo-hydro-chemo-mecanique des enceintes de confinement nucleaire en beton arme-précontraint. PhD Thesis, Universite de Toulouse, Universite Toulouse III - Paul Sabatier, France, 2017.